Many-body wave functions approximated by the superposition of spin-projected nonorthogonal Slater determinants in the resonating Hartree-Fock method

Norikazu Tomita
Institute of Materials Structure Science, 1-1 Oho, Tsukuba, Ibaraki 305, Japan
(Received 5 June 2003; revised manuscript received 14 October 2003; published 29 January 2004)

A resonating Hartree-Fock (Res-HF) method is revisited and improved by the complete spin projection for the interacting Fermion system. This method approximates a many-body wave function by the superposition of nonorthogonal Slater determinants (S-dets). The nonorthogonality of the S-dets makes it possible to describe the large quantum fluctuations efficiently, since each S-det naturally includes the full-electron-excitation effects from other S-dets. The molecular orbitals in every S-det, as well as the superposition coefficients, are variationally determined. So far, however, the spin contamination, caused by the conventional half-projection, has been a serious obstacle to obtain the accurate wave functions for large-size fermion systems, especially in the intermediate and large correlation regimes. In this paper, we apply the complete spin projection method to the Res-HF calculations. As an example, the improved Res-HF method is applied to the one-dimensional Hubbard model. It will be shown that the complete spin projection improves the Res-HF wave functions significantly. In fact, the correlation energies explained by the improved Res-HF method are better than those by the variational Monte Carlo method in all the correlation regimes. The correlation structures at arbitrary fillings are also well described by the improved Res-HF method.

DOI: 10.1103/PhysRevB.69.045110 PACS number(s): 71.15.−m, 71.10.Fd

I. INTRODUCTION

The development of the many-body theories which can describe the large quantum fluctuations in the interacting fermion systems has been one of the central problems in both the condensed matter and particle physics. For example, nuclei in the transition region between the spherical and largely deformed shapes, or the low-dimensional interacting electron systems are not described by the simple Hartree-Fock (HF) approximation, due to the large quantum fluctuations. Especially, since the discovery of the attractive materials, showing the high-temperature superconductivity or colossal magnetic resistance, it has been becoming more important to clarify the electron correlation effects in the condensed matters.

For small clusters, we can apply the exact diagonalization methods, such as the Lanczos,[1] valence bond,[2,3] and full configuration interactions (CI). However, the exact calculations are not applicable to large systems having more than 20 particles.To understand the bulk properties of the electron correlations, the real-space density-matrix renormalization group (DMRG) method has been developed,[4] but this method is applicable only to the one-dimensional (1D) or quasi-1D systems. On the other hand, for the infinite-dimensional system[5] or the system with the large orbital degeneracies,[6] the dynamical mean-field theory is applicable. However, this theory neglects the nonlocal fluctuation effects which will be important in the real finite-dimensional systems. A quantum Monte Carlo (QMC) simulation[7] is another alternative, but in the interacting fermion system, the QMC method often suffers the famous negative sign problem, where the probability to update a configuration becomes negative. The sign problem restricts the application of the QMC method. Recently, the momentum-space DMRG method has been developed.[8–10] This method is promising, since it is applicable to higher dimensions. However, at present, its accuracy becomes worse as the system size is increased or the interaction is increased. So far, only the variational Monte Carlo (VMC) method is applicable to the large and any-dimensional systems.[11] Therefore, we still need more theories, which are tractable and applicable to arbitrary interacting fermion systems.

In this paper, we revisit to a variational method called the resonating HF (Res-HF) approximation, originally developed by Fukutome.[12] This method approximates a many-body wave function by the superposition of the nonorthogonal Slater determinants (S-dets). In the early stage, a Res-HF wave function is constructed by optimizing only the superposition coefficients.[13,14] Then, the tractable orbital optimization method was developed by Ikawa *et al.*[15] Thus, now, the orbitals of every S-det, as well as the superposition coefficients, are variational determined in the Res-HF calculations. So far, the Res-HF method has been applied to the 1D half-filled Hubbard system, where we have the exact Lieb-Wu solutions.[16] In these previous calculations,[13–15] it was shown that the Res-HF approximation gives a reasonable agreement with the exact result in the correlation energy and correlation structures, up to $N=20$. However, when we applied this method to large-size fermion systems, we had a serious problem of the spin contamination in the Res-HF wave function, which makes the accuracy worse. This was due to the incomplete spin projection by a half-projection method, which can eliminate only odd (or even) spin contributions from the generating S-dets. As a result, the Res-HF method has been applied only to a small molecule[17] and nuclei.[18]

To overcome the problem, in this work, we apply the complete spin projection method proposed by Igawa[19] to the Res-HF calculations. It will be shown that the resonating of the completely spin-projected S-dets makes a much better wave function than the conventional one with the half-

projection. As a demonstration, the improved Res-HF method is applied to the 1D Hubbard model. It will be shown that the improved Res-HF wave function with the complete spin projection describes both the correlation energy and correlation structure much better than the previous one with the half-projection at any filling. In fact, we will show that the improved Res-HF method can describe more correlation energies than the VMC method in all the correlation regimes.

This paper is organized as follows. In Sec. II, the Res-HF method is introduced. We briefly review the complete spin-projection method employed in the present work. In Sec. III, the Res-HF method is applied to the 1D Hubbard model. We will show that this method gives very accurate wave functions in all the correlation regimes at any filling. Finally, a summary is given in Sec. IV.

II. METHOD

Here, let me review the basic idea on the Res-HF method. The most straightforward variational method, which can explain some of the electron correlations, is an unrestricted Hartree-Fock (UHF) approximation,[20] in which the ground state is described by a broken-symmetry S-det, here denoted by $|\phi_g\rangle$. As different correlation structures cause different broken symmetries, we can directly know the correlation structure through the UHF S-det. A spin-density wave (SDW) in the lattice fermion system is one example, which breaks the translation symmetry.

However, such a single S-det is not sufficient to describe the large quantum fluctuations. We need a multiconfigurational theory which can efficiently describe the electron correlation effects. Here, the important property of the nonlinear UHF equation is that it has various low-energy excited states, denoted by $|\phi_{e1}\rangle$, $|\phi_{e2}\rangle$,*etc.*, which have the large off-diagonal resonance elements with both the UHF ground state ($\langle\phi_{e1}|H|\phi_g\rangle$, etc.) and other excited states ($\langle\phi_{e1}|H|\phi_{e2}\rangle$, etc.), where H represents a many-body Hamiltonian. As the resonance of these UHF ground and excited states could stabilize the many-body states, the Res-HF method starts its many-body wave function with the superposition of the nonorthogonal UHF S-dets, such as

$$|\Psi\rangle=\sum_{n=1}^{N_S} C_n \sum_S P^S P^G |\phi_n\rangle. \tag{1}$$

Here, N_S represents the number of constituting S-dets. Then, the molecular orbitals (MO) of all the constituting S-dets are optimized to lower the Res-HF energy $\langle\Psi|H|\Psi\rangle$. In the following sections, we review the symmetry projection as well as the orbital optimization.

A. Peierls-Yoccoz projection

Since the S-dets constituting the Res-HF wave function can have different correlation structures, we have to adopt the symmetry projections for the constituting S-dets to recover the original symmetry of the system. Here, as an example, let us assume that the system belongs to the symmetry group G and $|\phi\rangle$ is a broken-symmetry S-det. G's elements p, which satisfy

$$|p\phi\rangle=|\phi\rangle, \tag{2}$$

constitute the subgroup G_ϕ of G. Then, for the elements s of the right coset G/G_ϕ, we find that

$$|s\phi\rangle\neq|\phi\rangle, \tag{3}$$

except for $s=1$. These $|s\phi\rangle$ are degenerate broken-symmetry S-dets and the set of $\{|s\phi\rangle\}$ is called the Goldstone set of $|\phi\rangle$. Peierls and Yoccoz[21] have proved that the original symmetry is recovered by the resonance of the degenerate Goldstone set. In the following, to recover the translation and inversion symmetries of the system, we apply the Peierls-Yoccoz projection to the constituting S-dets. P^G in Eq. (1) represents this Peierls-Yoccoz projection.

B. Complete spin projection

Now, we briefly review the complete spin projection of the S-dets.[19,22] Here, for convenience, we focus on the projection on the singlet states, since the ground state of the 1D Hubbard system, we study in the following section, is singlet.[23] In the Res-HF method, we need to calculate the matrix elements between nonorthogonal S-dets, such as

$$X(u,v)=\langle v|\hat{X}|u\rangle, \tag{4}$$

where $\hat{X}$ is an operator which is invariant for the spin rotation. As we are considering the singlet states, the number of up-spin electrons is equal to that of down-spin electrons ($n_\uparrow=n_\downarrow=N_e/2$). In this case, all the constituting S-dets satisfy

$$S_z|u\rangle=M|u\rangle, \tag{5}$$

$$M=0. \tag{6}$$

On the other hand, these S-dets are constituted of different eigenstates of S^2, such as

$$S^2|u\rangle=\sum_{j=0}^{j_{max}} j(j+1)|u_{j,M=0}\rangle,$$
$$j_{max}=min(N_e/2,N-N_e/2), \tag{7}$$

where N represents the total number of orbitals. As a result, the matrix element becomes

$$X(u,v)=\sum_{j=0}^{j_{max}} \langle v_{j,0}|\hat{X}|u_{j,0}\rangle. \tag{8}$$

The problem is how we can extract the contribution of the singlet states, given by

$$X(u,v)_0=\langle v_{0,0}|\hat{X}|u_{0,0}\rangle. \tag{9}$$

In this work, we employ the different orbitals for different spins for the constituting S-dets. Then, the S-det $|u\rangle$ is characterized by a matrix u, such as

$$u=\begin{pmatrix} u_1 & 0 \\ 0 & u_2 \end{pmatrix}, \tag{10}$$

where both u_1 and u_2 are $N\times N$ matrices, and their elements show the molecular orbital coefficients (MOC) for the up-spin and down-spin states, respectively.

Now, let us make the spin rotation for the S-det $|u\rangle$ with the Eulerian angles $(0,\beta,0)$, such as

$$R(\beta)|u\rangle = \left| \begin{pmatrix} \cos\frac{\beta}{2}u_1 & -\sin\frac{\beta}{2}u_2 \\ \sin\frac{\beta}{2}u_1 & \cos\frac{\beta}{2}u_2 \end{pmatrix} \right\rangle = \sum_{j=0}^{j_{max}} \sum_{k=-j}^{j} |u_{j,k}\rangle D_k^j(\beta). \tag{11}$$

We should note that the projected S-det has general spin orbitals. In the first line of Eq. (11), the rotated S-det is represented by the MOC matrix. Then, the matrix element of $\hat{X}$ becomes

$$X(\beta) = \langle v|\hat{X}R(\beta)|u\rangle = \sum_{j=0}^{j_{max}} \langle v_{j,0}|\hat{X}|u_{j,0}\rangle D_0^j(\beta) = \sum_{j=0}^{j_{max}} X_j p_j(\cos(\beta)), \tag{12}$$

where

$$X_j = \langle v_{j,0}|\hat{X}|u_{j,0}\rangle, \qquad p_j(\cos(\beta)) = D_0^j(\beta). \tag{13}$$

Here, the function $p_j(x)$ corresponds to the Jacobi polynomial of degree j,[24] and is given by

$$p_j(x) = \frac{1}{2^j}\sum_{k=0}^{j}\binom{j}{k}^2 (x-1)^{j-k}(x+1)^k. \tag{14}$$

It should be noted that we can directly obtain the matrix element $X(\beta)$, according to the formulas introduced in the following section. Eventually, by calculating $X(\beta)$ at different β's, we can make the simultaneous equations for X_j. By defining a matrix $\mathbf{G}$ and vectors $\mathbf{X}$ and $\mathbf{Y}$, such as

$$(\mathbf{G})_{i,j} = p_j(\cos(\beta_i)), \qquad (\mathbf{X})_j = X_j, \qquad (\mathbf{Y})_i = X(\beta_i), \tag{15}$$

Eq. (12) becomes

$$\mathbf{Y} = \mathbf{G}\mathbf{X}. \tag{16}$$

By reversing Eq. (16), we obtain

$$\mathbf{X} = \mathbf{G}^{-1}\mathbf{Y}. \tag{17}$$

From Eq. (17), we can select all the possible spin contribution, not only the singlet contribution but also higher-spin contributions. In actual calculations, Igawa has proved that if we employ zeros of Jacobi polynomial of degree i for β's, such as

$$p_i(\cos(\beta)) = 0, \tag{18}$$

we can eliminate the high-spin components up to $j = 2i-1$.[19] Therefore, for N-orbital system, $i = N/4+1$ is enough to extract the singlet-state component, given by Eq. (9), from Eq. (12). In this work, we set $i=8$ for $N=30$ systems and $i=13$ for $N=50$ systems, which eliminate the high-spin components up to $j=15$ and $j=25$, respectively. Therefore, they give the exactly singlet contributions for $N=30$ and $N=50$ systems, respectively. P^S in Eq. (1) represents this spin projection.

So far, the singlet Res-HF wave function was approximately constructed by the half-projection,[15,25] which only eliminates odd-spin components from Eq. (12). This half-projection is obtained by setting β at 0 and π. Then, $D_0^j(\beta)$ becomes

$$D_0^j(0) = 1, \qquad D_0^j(\pi) = (-1)^j. \tag{19}$$

As a result, Eq. (12) becomes

$$X(0) = X_0 + X_1 + X_2 + X_3 + \cdots, \tag{20}$$

$$X(\pi) = X_0 - X_1 + X_2 - X_3 + \cdots. \tag{21}$$

By adding Eqs. (20) and (21), we obtain

$$\frac{1}{2}[X(0)+X(\pi)] = X_0 + X_2 + \cdots. \tag{22}$$

Thus, the half-projection, given by

$$\frac{1}{2}(\langle v|XP^S(\pi)|u\rangle + \langle v|X|P^S(0)|u\rangle), \tag{23}$$

still has the spin contamination due to the even-spin states $(j=2,4,\ldots)$.

We will show that the complete spin projection, employed in this study, improves the accuracy of the Res-HF method significantly, compared to the half-projection method.

C. Res-HF equation

Here, we review the Res-HF procedure which determines the MO sets and superposition coefficients simultaneously.[12] A many-body Hamiltonian is generally given by

$$H = \sum_{\langle i,j\rangle} h_{j,i}a_j^\dagger a_i + \frac{1}{2}\sum_{i,j,k,l}\langle ki|lj\rangle a_k^\dagger a_l^\dagger a_j a_i, \tag{24}$$

where the spin direction is included in the indices i,j,k,l. First, the overlap between two S-dets is written as

$$\langle u|v\rangle = \det(z), \qquad z = u^\dagger v, \tag{25}$$

where u and v represent the MOC matrices of $|u\rangle$ and $|v\rangle$, respectively, defined by Eq. (10). On the other hand, the matrix element of a pair-particle operator between two S-dets is given by

$$\langle u|a_j^\dagger a_i|v\rangle = W(u,v)_{ij}\det(z), \tag{26}$$

where $W(u,v)$ is called the interstate density matrix and is explicitly given by

$$W(u,v)_{ij} = (vz^{-1}u^\dagger)_{ij}. \tag{27}$$

Then, the matrix element of a two-body product of pair-particle operators between two S-dets is given by

$$\langle u|a_k^\dagger a_l^\dagger a_j a_i|v\rangle = (W_{ik}W_{jl} - W_{il}W_{jk})\det(z). \tag{28}$$

Thus, the matrix element of the Hamiltonian between two S-dets is written as

$$\langle u|H|v\rangle = H[W(u,v)]\det(z),$$

$$H[W(u,v)] = \sum_{\langle i,j\rangle} h_{j,i}W_{ij} + \frac{1}{2}\sum_{i,j,k,l}[ki|lj]W_{ik}W_{jl},$$

$$[ki|lj] = \langle ki|lj\rangle - \langle kj|li\rangle. \tag{29}$$

As the Res-HF wave function is formally represented by

$$|\Psi\rangle = \sum_f |u_f\rangle c_f, \tag{30}$$

the normalization condition is given by

$$\langle\Psi|\Psi\rangle = \sum_{fg}\langle u_f|u_g\rangle c_f^* c_g = \sum_{fg}\det(z_{fg})c_f^* c_g = 1. \tag{31}$$

On the other hand, the energy expectation value is given by

$$\langle\Psi|H|\Psi\rangle = \sum_{fg}\langle u_f|H|u_g\rangle c_f^* c_g = \sum_{fg} H[W_{fg}]\det(z_{fg})c_f^* c_g, \tag{32}$$

where W_{fg} is the interstate density matrix of $|u_f\rangle$ and $|u_g\rangle$.

Now, $|u_f\rangle$'s and c_f's are determined by the variation of the Lagrangian

$$L = \langle\Psi|H|\Psi\rangle - E\langle\Psi|\Psi\rangle = \sum_{fg}\{H[W_{fg}] - E\}\det(z_{fg})c_f^* c_g, \tag{33}$$

where E is the Lagrange multiplier to secure the normalization condition and also has the meaning of the energy of the state $|\Psi\rangle$.

From the variation of this Lagrangian with respect to c_f^*, we obtain

$$\sum_g \{H[W_{fg}] - E\}\det(z_{fg})c_g = 0. \tag{34}$$

This is called the Res-HF CI (configuration interaction) equation. Once we have the set of S-dets, we can determine their superposition coefficients c_f's by this Res-HF CI equation.

Now, let us derive the variational equation to determine $|u_f\rangle$'s, such as

$$\frac{\delta L}{\delta u_f^*} = 0. \tag{35}$$

First, we introduce several mathematical expressions, used for the derivation of Eq. (35). From Eq. (29), we obtain

$$\delta H(W) = F_{ij}(W)\,\delta W_{ji} = \mathrm{tr}(F\,\delta W),$$
$$F_{ij}(W) = \frac{\delta H(W)}{\delta W_{ji}} = h_{ij} + \sum_{lk}[ij|kl]W_{lk}. \tag{36}$$

Then, from Eq. (27), we obtain

$$\delta W = (\delta v)z^{-1}u^\dagger + v(\delta z^{-1})u^\dagger + vz^{-1}(\delta u^\dagger)$$
$$= D(1-W) + (1-W)\tilde{D},$$
$$D = vz^{-1}(\delta u^\dagger), \quad \tilde{D} = (\delta v)z^{-1}u^\dagger, \tag{37}$$

where we use

$$\delta z^{-1} = -z^{-1}(\delta z)z^{-1} = -z((\delta u^\dagger)v + u^\dagger(\delta v))z^{-1}. \tag{38}$$

On the other hand, the variation of the overlap between two S-dets is given by

$$\delta(\det(z)) = \mathrm{tr}(z^{-1}\delta z)\det(z) = \mathrm{tr}(D+\tilde{D})\det(z), \tag{39}$$

where we use the relationship between $\det(z)$ and its b-a cofactor, such as

$$D_{ba} = \frac{\delta}{\delta z_{ba}}\det(z) = (z^{-1})_{ab}\det(z). \tag{40}$$

Now, from Eqs. (33) and (36)–(38), we obtain

$$\delta L = \mathrm{tr}[\{(1-W)F + H - E\}D + \tilde{D}\{F(1-W) + H - E\}]\det(z). \tag{41}$$

Finally Eq. (35) becomes

$$\sum_g K_{fg}c_f c_g = 0,$$
$$K_{fg} = \{(1-W_{fg})F(W_{fg}) + H(W_{fg}) - E\}W_{fg}\det(z_{fg}). \tag{42}$$

This is called the Res-HF equation. Once we have the set of trial S-dets and their superposition coefficients, we can update the MOC of the S-det $|u_f\rangle$ according to Eq. (42). After updating all the S-dets, we go back to Eq. (34), determine the new superposition coefficients, and then update the orbitals of the S-dets again. By iterating these procedures, we can variationally determine the MO sets and superposition coef-

TABLE I. The ground state energies of the 1D half-filled and doped Hubbard systems. Res-HF(HP) and Res-HF ($i=8$) denote the Res-HF results with the half-projection and $i=8$ spin projection, respectively. The correlation energy explained by each method is denoted by κ (%).

		$N=N_e=30$	κ	$N=30,\ N_e=26$	κ	$N=30,\ N_e=22$	κ
	RHF	−23.2671		−26.1642		−26.8921	
	UHF	−23.4792	10.0				
U=2	Res-HF(HP)	−23.3206	97.0	−27.9920	98.2	−28.4227	98.6
	Res-HF($i=8$)	−25.3436	98.1	−27.9979	98.5	−28.4268	98.9
	Exact	−25.3835		−28.0253		−28.4441	
	RHF	−8.2671		−14.8975		−18.8254	
	UHF	−14.0732	64.8	−17.3756	35.0	−20.1328	23.4
U=4	Res-HF(HP)	−16.5992	92.9	−21.3820	91.5	−24.0803	94.2
	Res-HF($i=8$)	−17.0542	97.5	−21.5720	94.1	−24.1582	95.5
	Exact	−17.2335		−21.9868		−24.4057	
	RHF	21.7329		−7.6358		−2.6921	
	UHF	−7.8329	93.6	−11.2049	79.5	−14.9299	69.3
U=8	Res-HF(HP)	−9.0678	97.6	−14.7040	94.2	−19.0474	92.6
	Res-HF($i=8$)	−9.5378	99.0	−15.4059	97.2	−19.5552	95.5
	Exact	−9.8387		−16.0761		−20.3462	

ficients simultaneously.[12] In this work, we have converged the Res-HF wave functions and its energy functionals up to 10^{-6}.

The orbital optimization procedure is quite important to obtain the accurate many-body state. In the conventional CI-based method, the single common orbital set is used for all the configurations. Therefore, it is almost impossible to incorporate the high-order electron-excitation effects from each configuration unless the system is very small. Such high-order electron-excitation effects become quite important in describing the strongly correlated fermion system. In the Res-HF method, different S-dets have different optimized orbital sets and they are nonorthogonal to each other. Therefore, each S-det can naturally include the full-electron-excitation effects from other S-det.

III. RESULTS AND DISCUSSION

Now, we apply the Res-HF method to the 1D single-band Hubbard model, where we have the exact solutions for both the half-filled and doped cases.[16,26] The Hamiltonian is given by

$$H=-t\sum_{l,\sigma}^{N}\left(a_{l,\sigma}^{\dagger}a_{l+1,\sigma}+a_{l+1,\sigma}^{\dagger}a_{l,\sigma}\right)+U\sum_{l}^{N}n_{l,\uparrow}n_{l,\downarrow}, \tag{43}$$

where N represents the system size. In the following, all the energies are normalized by the transfer energy t. In this study, the periodic boundary condition is imposed. Therefore, the system has the D_N symmetry. In the following, we show the Res-HF results mainly for $N=30$ and 50 systems. In these cases, the ground state has the ${}^1A_1$ symmetry, and therefore, the Res-HF wave function is explicitly represented by

$$|\Psi\rangle=\sum_{n=1}^{N_S}C_n\sum_{m=0}^{N-1}P^S T^m(1+R)|\phi_n\rangle, \tag{44}$$

where the operator T makes the translation of the S-det by one site, while R represents the C_2 rotation in the D_N symmetry group. The operation of T and R corresponds to the Peierls-Yoccoz projection. P^S represents the $i=8$ (for $N=30$) or $i=13$ (for $N=50$) spin projection introduced in the previous section. Thus, for each generating S-det $|\phi_n\rangle$, 2 (C_2 rotation) $\times N$ (translation) $\times i$ (spin-projection) symmetry projections are operated. As a result, the symmetry-recovered Res-HF wave function consists of $2Ni\times N_S$ S-dets. In the following calculations, $N_S=30$ generating S-dets are used.

In Table I, we show the ground-state energies of the 1D half-filled and doped Hubbard systems, having $N=30$ sites. Here, N_e represents the number of electrons. RHF denotes the restricted HF state,[27] which satisfies the full symmetries of the system and is the reference state for the perturbation theory. For comparison, the UHF energies are also shown in this table except for $N_e=26$ and 22 at $U=2$, where no stable UHF solutions were obtained. In this table, we also compare the ground-state energies by the complete spin-projection method, denoted by Res-HF ($i=8$), to those by the half-projection method, denoted by Res-HF (HP). The exact solutions are obtained by the Lieb-Wu equations,[16,26] and κ denotes the ratio of the correlation energy explained by the Res-HF or UHF wave function, which is defined by

$$\kappa=100\times\frac{\mathrm{E(Res\text{-}HF\ \ or\ \ UHF)}-\mathrm{E(RHF)}}{\mathrm{E(Exact)}-\mathrm{E(RHF)}}. \tag{45}$$

It is remarkable that for both the half-filled and doped systems, the Res-HF wave functions can describe more than 91% of the correlation energies in all the correlation regimes.

TABLE II. The ground-state energies and $\langle S^2 \rangle$ for $N=N_e=50$. Res.-HF(HP) denotes the Res-HF result with the half-projection while Res-HF($i=13$) denotes the result with $i=13$ spin projection. The VMC results are taken from Ref. 1.

		Energy	κ(%)	$\langle S^2 \rangle$
	RHF	−38.7039		
	UHF	−39.1294	12.0	
	VMC		≈87	
U=2	ResHF(HP)	−41.8565	89.0	1.72
	ResHF($i=13$)	−41.9535	91.8	0
	Exact	−42.2443		
	RHF	−13.8039		
	UHF	−23.4553	64.4	
	VMC		≈92	
U=4	ResHF(HP)	−26.9727	88.5	7.42
	ResHF($i=13$)	−27.9633	94.4	0
	Exact	−28.6993		
	RHF	36.2961		
	UHF	−12.3048	92.3	
	VMC		≈96	
U=8	ResHF(HP)	−14.4838	96.4	12.8
	ResHF($i=13$)	−15.6422	98.6	0
	Exact	−16.3842		

So far, the Res-HF method has been applied only to the half-filled Hubbard system, and this is the first result showing that this method works well also for the doped systems. Table I also shows that the complete spin projection makes the Res-HF wave functions significantly better than the half-projection especially at $U=4$ and 8.

Recently, the momentum-space DMRG (MSDMRG) method has been developed and applied to the 1D Hubbard model.[9,10] In the case of $N=N_e=32$, they have obtained -33.2008 and -26.8016 for the ground-state energies at $U=1$ and $U=2.0$, respectively, while the exact energies are -33.2152 and -27.0183, respectively.[10] For comparison, we have calculated the Res-HF wave functions also for $N=N_e=32$. In this case, the ground state has the $^1B_1$ symmetry. Then, the obtained Res-HF energies are -33.2128 and -26.9556 at $U=1$ and $U=2.0$, respectively. Thus, the Res-HF method can describe more correlation energy than the MSDMRG method, though the MSDMRG method might be improved by increasing the number of the density-matrix eigenstates which are kept in the renormalization procedure.

Then, in Table II, we compare the complete ($i=13$) spin-projection method to the half-projection method, for $N=N_e=50$ Hubbard systems. At $U=2$ and 4, the half-projection method can explain only less than 90% of the correlation energies. From this table, we can see that the complete spin projection method improves the Res-HF wave functions significantly in all the correlation regimes. In the half-projection method, the expectation values of S^2 are far from zero in all the correlation regimes. The spin contamination was a serious problem to construct an accurate Res-HF wave function for the large-size system. Now, however, we can see that by the $i=13$ spin projection, the spin contamination is completely eliminated, and the Res-HF wave functions are significantly improved for the $N=N_e=50$ systems.

Here, let us compare the present results to the VMC ones. In Table II, we also show the ratios of the correlation energies explained by the VMC method[11] for $N=N_e=50$. We can see that the Res-HF method with the complete spin projection can explain more correlation energies than the VMC method in all the correlation regimes.

Then, in Fig. 1, we show the N_S dependence of the correlation energy explained by the Res-HF wave function at $U=4$. Black circles and triangles represent the N_S dependence of κ by the complete spin projection method for $N=30$ and $N=50$ half-filled Hubbard systems, respectively, while circles and triangles represent κ by the half-projection method for these systems. For comparison, the UHF results are also denoted by white square and diamond for $N=30$ and $N=50$ systems, respectively. In the case of $N_s=1$, the Res-HF wave function corresponds to the projected HF state. Figure 1 shows that even with $N_s=1$, the Res-HF wave functions with the complete spin projection describe more than 90% of the correlation energies for both $N=30$ and $N=50$ systems. This result, as well as the whole N_S-dependence, indicate that the orbital optimization with the complete symmetry projections is very important to construct the accurate wave functions.

From Fig. 1, we can see that as the system-size is increased, we need a larger number of S-dets to maintain the quality of the Res-HF wave function. On the other hand, Fig. 1 also shows that the quality of the Res-HF wave function is improved with the increase of the number of S-dets. Although it might be difficult to extrapolate the Res-HF energies at $N_S \to \infty$ from Fig. 1, the Res-HF approximation coin-

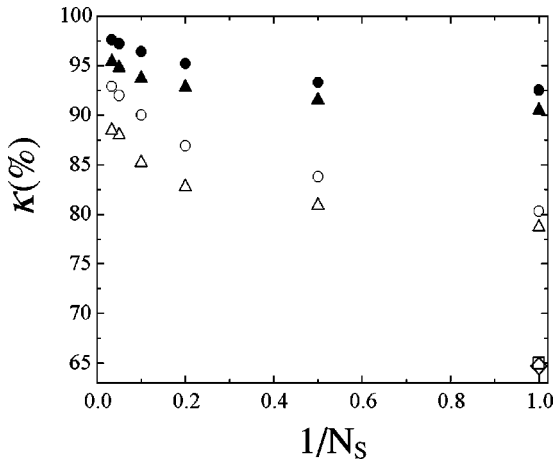

FIG. 1. N_s-dependence of the correlation energies explained by the Res-HF wave functions at $U=4$. Black circles and triangles represent the N_S dependence of κ by the complete spin-projection method for $N=30$ and 50 half-filled Hubbard systems, respectively, while white circles and triangles represent κ by the half-projection method for those systems. A white square and diamond denote the UHF results for $N=30$ and 50 systems, respectively.

cides with the exact coherent-state representation[28] of the fermion state vector $|\Psi\rangle$ in the limit of large N_s, such as

$$|\Psi\rangle=\int U(u)|\phi\rangle\langle\phi|U^{\dagger}(u)|\Psi\rangle du=\int |u\rangle\langle u|\Psi\rangle du. \tag{46}$$

Since the MOC matrix of a S-det, given by Eq. (10), belongs to the $U(2N)$ group, the integration, in Eq. (46), represents a normalized group integration on $U(2N)$. $U(u)$ is a representation of the $U(2N)$ group, defined by

$$U(u)=e^{\gamma_{ij}a_i^{\dagger}a_j}. \tag{47}$$

Here, the dummy index convention is used to sum up the repeated indices. γ_{ij} is a $2N\times 2N$ antihermitian matrix, which satisfies

$$\gamma=(\gamma_{ij}),$$
$$\gamma^{\dagger}=-\gamma. \tag{48}$$

Then, we obtain

$$U(u)a_i^{\dagger}U(u)^{\dagger}=a_j^{\dagger}u_{ji}, \quad U(u)a_iU(u)^{\dagger}=a_ju_{ji}^{*}, \tag{49}$$

where $u=(u_{ij})$ is the $U(2N)$ matrix, given by

$$u=e^{\gamma}, \quad \gamma=(\gamma_{ij}), \quad uu^{\dagger}=u^{\dagger}u=1. \tag{50}$$

In Eq. (46), we have used this $U(2N)$ canonical transformation, which transforms a given N_e-particle S-det $|\phi\rangle$ to an arbitrary N_e-particle S-det $|u\rangle$, such as

$$U(u)|\phi\rangle=|u\rangle. \tag{51}$$

This is called the Thouless transformation.[29] In general, $|u\rangle$ is nonorthogonal to $|\phi\rangle$. As a result, Eq. (46) indicates that the arbitrary fermion state vector is exactly described by the superposition of the nonorthogonal S-dets. Thus, the Res-HF wave function corresponds to the discretized expression for the exact coherent-state representation, defined by Eq. (46).

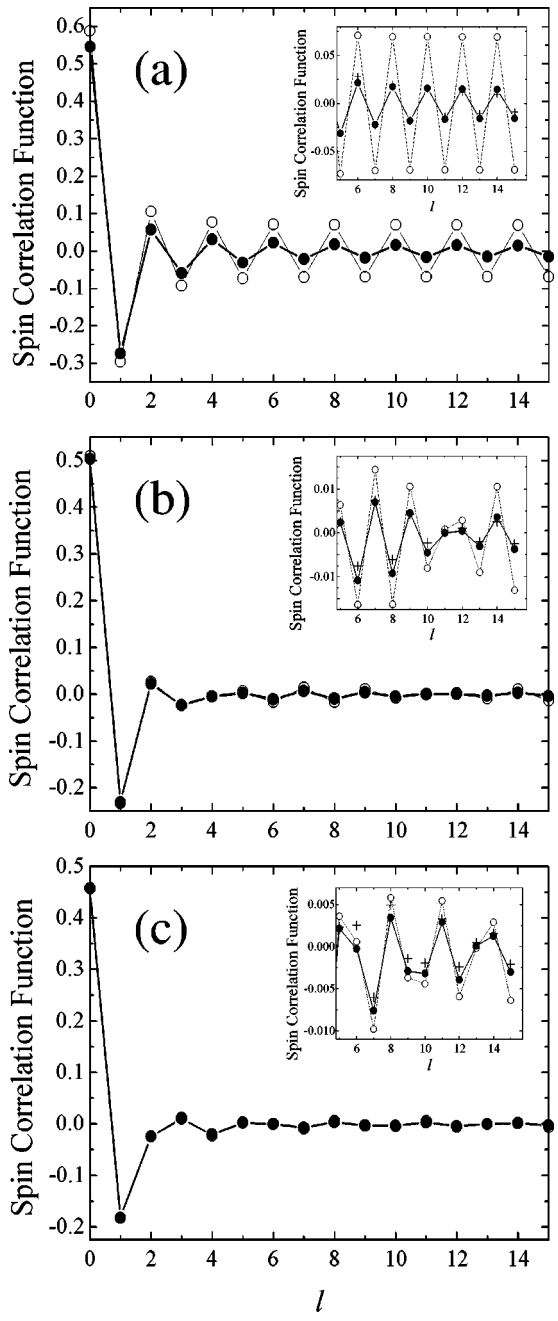

FIG. 2. Spin correlation functions for $N=N_e=30$ (a), $N=30$, and $N_e=26$ (b), and $N=30$ and $N_e=22$ (c). Black circles represent the Res-HF results with the complete spin projection, while white circles represent those with the half-projection. The close-up of the long-range behavior is shown in the inset of each figure, where the crosses show the exact long-range behavior normalized at $L_S(5)$.

Next, we show in Fig. 2 the spin correlation functions of the Res-HF wave functions for $U=4$. Black and white circles represent the correlation functions obtained by the complete spin projection and half-projection methods, respectively. The exact long-range exponent of the spin correlation function is given by[30,31]

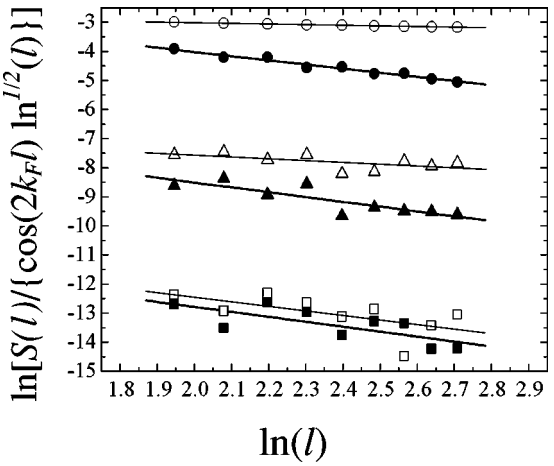

FIG. 3. The exponents of the long-range spin correlation functions. Black circles, triangles, and squares denote the log-scaled long-range structures obtained by the complete spin-projection method for $(N,N_e)=(30,30)$, $(30,26)$, and $(30,22)$, respectively, where the exponents are given by thick lines. White circles, triangles, and squares denote those by the half-projection method, whose exponents are given by thin lines.

$$L_S(l)=\langle \mathbf{S}(0)\cdot\mathbf{S}(l)\rangle \propto \cos(2k_F l) l^{-1-\alpha}\ln^{1/2}(l), \quad (52)$$

where α depends on U and fillings. From Ref. 30, we obtain $\alpha=0.50$, 0.66, and 0.72 for $N_e/N=1.0$, 0.87, and 0.73, respectively. In the inset of Fig. 2, the crosses show these exact long-range behaviors, which are normalized at $L_S(5)$ of each Res-HF result.

In Fig. 2(a), I show $L_S(l)$ for $N=N_e=30$. The long-range behaviors are enlarged in the inset, where, as mentioned above, the crosses show the exact behaviors. We can see the spin correlation structure is well described by the Res-HF wave function with the complete spin projection. On the other hand, in the half-projection method, the long-range components decay much more slowly than the exact behavior. This is due to the spin contamination caused by the half-projection method.

In Figs. 2(b) and 2(c), the spin correlation functions for the doped systems are shown. We can see that the Res-HF wave functions with the complete spin projection describe the exact long-range behaviors of the spin correlation functions much better than the conventional ones with the half-projection, also for the doped systems.

Figure 3 shows the log-scaled long-range behaviors of the spin correlation functions, derived from Fig. 2. Black and white symbols represent the spin correlation functions obtained by the complete spin projection and half-projection methods, respectively. Circles, triangles, and squares denote the correlation functions for $(N,N_e)=(30,30)$, $(30,26)$, and $(30,22)$, respectively. To see the long-range exponents clearly, vertical axis is shifted by -3.0 for $(N,N_e)=(30,26)$, and -7.5 for $(30,22)$. From Fig. 3, the Res-HF calculations with the complete spin projection, denoted by thick lines, result in the long-range exponents of -1.43, -1.65, and -1.69 for $(N,N_e)=(30,30)$, $(30,26)$, and $(30,22)$, respectively, which agree reasonably with the exact exponents of -1.5, -1.66, and -1.72, respectively. On the other hand, the half-projection method gives the exponents, denoted by thin lines, -0.23, -0.62, and -1.56, which are largely different from the exact values. Thus, the complete spin projection improves the Res-HF wave functions significantly.

As the 1D Hubbard system does not have a real long-range order, $N=30$ is large enough to see the agreement of the Res-HF results with the exact ones. For much larger systems, the absolute values of the long-range correlation functions become so small that it would be quite complicated to see the agreement of the numerical results with the exact ones quantitatively.

Then, we show the optimized S-dets. Though the orbital optimization modifies the starting UHF S-dets, we can often interpret the quantum fluctuations in terms of the UHF-based picture, by seeing the order parameters of the optimized S-dets.

So far, it has been complicated to show explicitly what makes the quantum fluctuations in the correlated electron systems. The Res-HF method gives a simple but interesting physics on the quantum fluctuations.

Here, the S-det is represented by its charge density (CD) and spin density (SD), defined as

$$\begin{aligned} CD(l)&=1.0-(n_{l,\uparrow}+n_{l,\downarrow})=NCD(l)+(-1)^l ACD(l),\\ SD(l)&=(n_{l,\uparrow}-n_{l,\downarrow})=NSD(l)+(-1)^l ASD(l), \end{aligned} \quad (53)$$

where the net and alternating components of the CD (SD) are denoted by NCD (NSD) and ACD (ASD), respectively.

In the half-filled Hubbard system, the optimized S-dets have no CD components. Therefore, in Fig. 4(a), we show only the SD components of the typical optimized S-dets for $N=N_e=30$. In this half-filled system, the most important element of the quantum fluctuations is an SDW neutral soliton, which reverses the phase of the ASD and has only the NSD. The S-dets shown in Figs. 4(a) 1–3 contain a soliton pair, whose distance is different from each other. The superposition of such a soliton pair with different distance can be interpreted as the breathing or vibrational motion of the two solitons. Similarly Figs. 4(a) 4–6 show the breathing motion of the two soliton pairs. On the other hand, as mentioned in Sec. II, these solitons are transferred site-by-site to recover the spatial translation symmetry. Thus, the quantum fluctuations in the half-filled system can be interpreted as the breathing and translational motions of the neutral solitons. The present analysis is consistent with the previous discussion based on the half-projection method.[13–15]

On the other hand, there has been no such physical description for the doped Hubbard systems so far. This is the first trial to describe the quantum fluctuations in the doped Hubbard systems in terms of the Res-HF picture. In the doped system, the most important element is an SDW charged soliton, which also reverses the phase of the ASD but has only the NCD. In Fig. 4(b), we show the typical S-dets for the doped Hubbard system with $N=30$ and $N_e=26$. Although the order parameters have complicated structures in the doped system compared to the half-filled case, we can see from Figs. 4(b) 1-4 that the breathing and translational motions of the charged solitons make the dominant

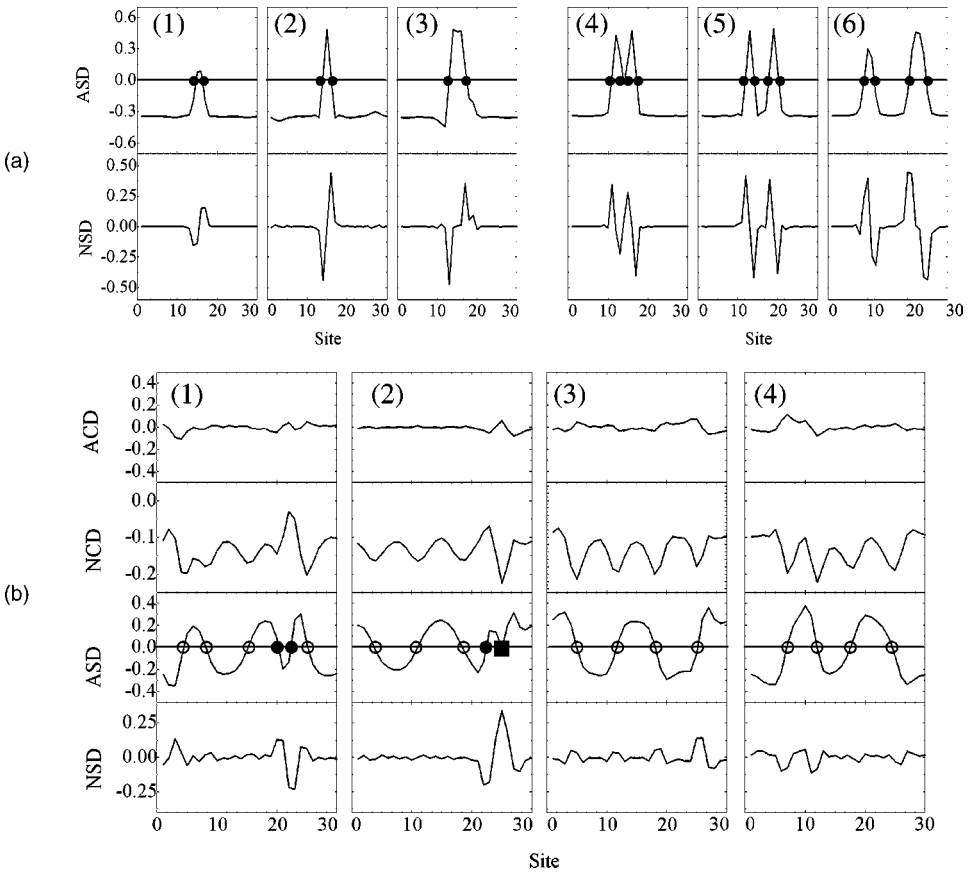

FIG. 4. Typical optimized S-dets generating the Res-HF wave functions for $N=N_e=30$ (a) and $N=30$ and $N_e=26$ (b). Black and white circles represent the SDW neutral and charged solitons, respectively, while a black square in (b) 2 represents a polaron, which makes a dip in the ASD and have both NSD and NCD.

quantum fluctuations in the doped 1D Hubbard system. In addition to these charged solitons, the 1D doped system has a defect called a polaron, which makes a dip in the ASD and has both NCD and NSD. In fact, we can see the polaron, denoted by a black square, in Fig. 4(b) 2. Therefore, a part of the quantum fluctuations in the doped system can be described as the translational motion of the polaron.

Thus, the Res-HF method gives the physical picture on the quantum fluctuations, that is, the large quantum fluctuations in the 1D Hubbard systems are described mainly as the vibrational and translational motions of the SDW neutral or charged solitons.

Finally, we comment on the present status of the Res-HF calculations. The system size, to which we can practically apply the Res-HF method by the α-CPU workstation, is about $N=70$ at present. As shown in Fig. 1, we need a larger number of S-dets to obtain the accurate Res-HF wave functions for larger systems. On the other hand, the computational time depends on $N_S^2\times N^3$.[15] Therefore, by using the parallel computer having 100 nodes, we will be able to extend the system size to about $N=200$, even if we have to double the number of S-dets to obtain the reliable Res-HF wave function. This application will be done in the near future.

IV. SUMMARY

We have revisited to the Res-HF method and shown that it could be a promising variational approach for the interacting fermion systems. The nonorthogonality of the generating S-dets enables us to describe the large quantum fluctuations efficiently, since each S-det naturally includes the full-electron-excitation effects from other S-dets. The complete spin projection method has been applied to the Res-HF calculations, to eliminate the spin contamination in the S-dets generating the Res-HF wave functions. We have shown that the complete spin projection is very important to improve the Res-HF wave function. In fact, it has been shown that both the correlation energies and correlation structures described by the Res-HF wave functions with the complete spin projection are much better than those with the half-projection. Then, we have shown, through the S-dets generating the Res-HF wave function, that the dominant quantum fluctuations in the 1D Hubbard systems are described as the vibrational and translational motions of the SDW neutral or charged solitons. Since the Res-HF method does not suffer any problems from the dimensionality and filling, it can be a powerful tool for the studies of the interacting fermion systems.

ACKNOWLEDGMENTS

This work was supported by NAREGI Nanoscience Project, Ministry of Education, Culture, Sports, Science and Technology, Japan. Numerical calculation in this work was partially supported by Yukawa Institute Computer Facility. The author would like to thank Dr. Michel A. Van Hove for his hospitality during the author's stay at Lawrence Berkeley National Laboratory. The author would also like to thank Professor A. Igawa for the valuable discussion on the spin projection in the Res-HF calculations.

[1] E. Dagotto and A. Moreo, Phys. Rev. D **31**, 865 (1985).
[2] Z.G. Soos and S. Ramasesha, Phys. Rev. B **29**, 5410 (1984).
[3] S. Mazumdar and S.N. Dixit, Phys. Rev. Lett. **51**, 292 (1983).
[4] S.R. White, Phys. Rev. Lett. **69**, 2863 (1992).
[5] For a review, see A. Georges, G. Kotliar, W. Krauth, and M.J. Rozenberg, Rev. Mod. Phys. **68**, 13 (1996).
[6] S. Florens, A. Georges, G. Kotliar, and O. Parcollet, Phys. Rev. B **66**, 205102 (2002).
[7] For a review, see *Quantum Monte Carlo Method in Condensed Matter Physics*, edited by M. Suzuki (World Scientific, Singapore, 1993).
[8] S.R. White, Phys. Rev. B **45**, 5752 (1992).
[9] T. Xiang, Phys. Rev. B **53**, 10 445 (1996).
[10] S. Nishimoto, E. Jeckelmann, F. Gebhard, and R.M. Noack, Phys. Rev. B **65**, 165114 (2002).
[11] H. Yokoyama and H. Shiba, J. Phys. Soc. Jpn. **56**, 3582 (1987).
[12] H. Fukutome, Prog. Theor. Phys. **80**, 417 (1988).
[13] S. Yamamoto, A. Takahashi, and H. Fukutome, J. Phys. Soc. Jpn. **60**, 3433 (1991).
[14] S. Yamamoto and H. Fukutome, J. Phys. Soc. Jpn. **61**, 3209 (1992).
[15] A. Ikawa, S. Yamamoto, and H. Fukutome, J. Phys. Soc. Jpn. **62**, 1653 (1993).
[16] E.H. Lieb and F.Y. Wu, Phys. Rev. Lett. **20**, 1445 (1968).
[17] N. Tomita, S. Ten-no, and Y. Tanimura, Chem. Phys. Lett. **263**, 687 (1996).
[18] S. Nishiyama, Nucl. Phys. A **576**, 317 (1994).
[19] A. Igawa, Int. J. Quantum Chem. **54**, 235 (1995).
[20] J.A. Pople and R. K Nesbet, J. Chem. Phys. **22**, 571 (1954).
[21] R.E. Peierls and J. Yoccoz, Proc. Phys. Soc., London, Sect. A **70**, 381 (1957).
[22] P.O. Löwdin, Phys. Rev. **97**, 1475 (1055).
[23] E. Lieb and D. Mattis, Phys. Rev. **125**, 164 (1962).
[24] I.S. Gradshteyn and I.M. Ryzhik, *Table of Integrals, Series and Products*, edited by A. Jeffrey (Academic Press, London, 1980).
[25] Y.G. Smeyers and L. Doreste-Suarez, Int. J. Quantum Chem. **15**, 33 (1973).
[26] K. Hashimoto, Int. J. Quantum Chem. **30**, 633 (1986).
[27] C.C.J. Roothaan, Rev. Mod. Phys. **32**, 179 (1960).
[28] A.M. Perlemov, Sov. Phys. Usp. **20**, 703 (1977).
[29] D.J. Thouless, Nucl. Phys. **21**, 225 (1960).
[30] H.J. Schulz, Phys. Rev. Lett. **64**, 2831 (1990).
[31] N. Kawakami and S.-K. Yang, Phys. Lett. A **148**, 359 (1990).